JGR Atmospheres

RESEARCH ARTICLE
10.1029/2019JD031742

Special Section:
Integrative Monsoon Frontal Rainfall Experiment

Diurnal Variation of Meiyu Rainfall in the Yangtze Plain During Atypical Meiyu Years

A. Q. Zhang[1,2,3], Y. L. Chen[1,2,3], S. N. Zhou[1,4], C. G. Cui[5], R. Wan[5], and Y. F. Fu[1]

[1]School of Earth and Space Sciences, University of Science and Technology of China, Hefei, China, [2]School of Atmospheric Science, Sun Yat-sen University, Zhuhai, China, [3]Southern Marine Science and Engineering Guangdong Laboratory (Zhuhai), Zhuhai, China, [4]Anhui Meteorological Observatory, Hefei, China, [5]Hubei Key Laboratory for Heavy Rain Monitoring and Warning Research, Institute of Heavy Rain, China Meteorological Administration, Wuhan, China

Key Points:
- The diurnal variation of Meiyu rainfall over the Yangtze Plain varies from year to year
- Meiyu precipitation over the Yangtze Plain in atypical Meiyu years showed two diurnal peaks in early morning and afternoon
- The diurnal variation of Meiyu rainfall is thought to be influenced by the southwesterly low-level water vapor flux

Correspondence to:
Y. F. Fu,
fyf@ustc.edu.cn

Citation:
Zhang, A. Q., Chen, Y. L., Zhou, S. N., Cui, C. G., Wan, R., & Fu, Y. F. (2020). Diurnal variation of meiyu rainfall in the yangtze plain during atypical meiyu years. *Journal of Geophysical Research: Atmospheres*, *125*, e2019JD031742. https://doi.org/10.1029/2019JD031742

Received 27 SEP 2019
Accepted 27 DEC 2019
Accepted article online 2 JAN 2020

Abstract The diurnal variation of precipitation reflects the influence of atmospheric heat and dynamic processes on the water cycle. Using multiple data sets, we carried out case studies and statistical analysis of the diurnal variation in Meiyu rainfall in atypical Meiyu years. Our results show that the morning precipitation was induced by strong southwesterly moisture transport and was mainly composed of stratiform pixels, whereas the precipitation occurring in the afternoon was mainly composed of convective pixels affected by updrafts. The diurnal variation in precipitation in the atypical Meiyu years appeared as a bimodal structure with peaks in early morning (06:30 LST) and afternoon (16:00 LST), which was different from the single morning peak (09:30 LST) in the normal Meiyu years and reported previously. Further research indicated that the morning peak is related to the low-level water vapor flux, whereas the afternoon peak is related to the local solar heating. In addition, the water vapor flux in the Yangtze Plain was characterized by strong morning and weak afternoon fluxes during both normal and atypical Meiyu periods. The diurnal variation in the low-level water vapor flux is thought to be influenced by the intensity of, and distance from, the subtropical high.

1. Introduction

Meiyu rainfall, also called Baiu in Japan and Changma in Korea, is the most pronounced spring-summer precipitation over East Asia (Xu et al., 2010). The start and end dates of the Meiyu period vary in different regions. The Meiyu period on the Yangtze Plain usually starts in mid-June and ends in mid-July (Tao & Ding, 1981). Despite the short duration of the Meiyu period, Meiyu rainfall accounts for a large proportion of the annual precipitation, exceeding 50% of the total precipitation on the Yangtze Plain in some years (Ding, 1992). Much research has been carried out to gain a better understanding of Meiyu rainfall with the aim of improving the prediction of heavy rainfall and reducing losses due to flooding (Li et al., 2019; Luo et al., 2013; Ninomiya & Akiyama, 1992; Ninomiya & Shibagaki, 2007; Sampe & Xie, 2010; Xu et al., 2018; Zhang et al., 2008; Zheng et al., 2008).

Diurnal variation is influenced by atmospheric heat and dynamic processes on the water cycle and is an important aspect of precipitation research (Yu & Li, 2016). In particular, diurnal variations in the summer monsoon precipitation over contiguous China have received much attention in recent years and significant regional differences have been reported (Chen et al., 2009a, 2009b; Li et al., 2010; Yu, Zhou, et al., 2007, Yu, Xu, et al., 2007; Zhou et al., 2008). For instance, summer precipitation over south and northeast China peaks in the late afternoon (Yu, Zhou, et al., 2007), which is consistent with most land areas worldwide (Nesbitt & Zipser, 2003). However, the peak time of summer precipitation in the Yangtze river valley shows a characteristic eastward propagation, with peak rainfall in the upper and middle reaches of the Yangtze river occurring at midnight and in the early morning, respectively (Chen et al., 2012; Yu, Zhou, et al., 2007). Summer precipitation in the lower reaches of the Yangtze valley has one diurnal peak in the early morning and another in the late afternoon (Yu, Zhou, et al., 2007). The different diurnal cycles of summer precipitations in the Yangtze valley are thought to be related to the eastward movement of clouds over the Tibetan Plateau (Asai et al., 1998; Chen et al., 2014; Wang et al., 2004; Zhang et al., 2019).

Although the Meiyu rainband has a close association with the seasonal advance and retreat of the East Asian summer monsoon (Chang et al., 2000; Sampe & Xie, 2010; Xue et al., 2018), the diurnal variations in Meiyu rainfall are different from summer precipitation in the Yangtze Plain (Geng & Yamada, 2007; Xue et al.,

2018). Using 8-year (1998–2005) Tropical Rainfall Measurement Mission precipitation radar reflectivity data, Geng and Yamada (2007) studied the diurnal variation of the Meiyu rainband and found that the precipitation radar reflectivity had a remarkable early morning peak in the Meiyu frontal region. The causes of the early morning peak in the Meiyu rainfall in the Yangtze Plain have been further investigated (Chen, Sha, et al., 2017; Xue et al., 2018). Chen, Sha, et al. (2017) presented numerical simulations of a heavy rainfall event on 11–16 June 1998 and suggested that the southwesterly nocturnal low-level jet acts as a mechanism for the transport of moisture and the formation of rainfall. Using the WRF-ARW model, Xue et al. (2018) performed a 6-day simulation of Meiyu precipitation over the Yangtze Plain and attributed the prominent peak in the morning rainfall to the diurnal cycle of clockwise rotation of low-level ageostrophic winds in the southwest of the Meiyu rainband. Thus, the ageostrophic wind is perpendicular to the geostrophic wind, which reduced the supply of moisture in the afternoon, whereas they are parallel and in same direction during early morning leading to the improved southwesterly moisture flux.

Previous work has laid a good foundation for recognizing the daily variation in Meiyu frontal precipitation. However, several features of Meiyu fronts, including the onset date and cessation date and the total amount of rainfall, significantly differ among different years (Ge et al., 2008; Li et al., 2019; Zhang et al., 2008). The duration and precipitation of the Meiyu period is affected by factors such as the subtropical high, the South Asian anticyclone, and the El Niño–Southern Oscillation (Ding, 1992; Li et al., 2019; Sun et al., 2010). For example, Ge et al. (2008) studied the duration and total rainfall of the Meiyu period in the Yangtze Plain from 1951 to 2000 and showed that the longest duration of the Meiyu period was 58 days, whereas the shortest duration was 7 days. The maximum rainfall reached 695 mm, 10 times the minimum rainfall (61 mm). The relationships between the diurnal cycles of Meiyu rainfall and the annual variations in the Meiyu fronts have not yet been determined. In particular, in atypical Meiyu years such as 2018, it is worth considering whether the diurnal cycle of Meiyu rainfall still showed an early morning peak. We therefore carried out case studies and statistical analysis on the diurnal variation of Meiyu rainfall in the atypical Meiyu years in comparisons to the previous works.

This paper contains seven sections. Section 2 describes the data and methods used in this research. The overall environmental circulation and precipitation during the atypical Meiyu periods are described in section 3. The two typical precipitation events that occurred during the Integrative Monsoon Frontal Rainfall Experiment (IMFRE) in 2018 are presented in sections 4 and 5. The diurnal variation in Meiyu precipitation in atypical Meiyu years is discussed in section 6. The final section is the discussion and conclusions.

2. Data and Methods

2.1. Data Sets

We used two different precipitation products, both available from the Precipitation Measurement Mission website (https://pmm.nasa.gov). The Global Precipitation Measurement (GPM) Integrated Multi-satellite Retrievals for GPM (IMERG) data set is a level 3 multisatellite precipitation data set. The IMERG data set provides combined precipitation estimates from satellite microwave sensors, satellite infrared-based observations, and rain gages at a time resolution of 30 min and a horizontal resolution of 0.1° × 0.1° (Hou et al., 2014). Based on the calculation time and usage data, the IMERG data set is divided into an early run, a late run, and a final run. The IMERG final run product used in this study was verified by. We used the IMERG final run product, which was verified by Tang et al. (2016), for statistically studying the diurnal variations of the precipitation in this work.

The GPM Dual-frequency Precipitation Radar (DPR) is the first space-borne dual-frequency radar system designed by the Japan Aerospace Exploration Agency and the National Aeronautics and Space Administration (NASA) and consists of Ka-band and Ku-band precipitation radar. The GPM 2ADPR precipitation product is a level 2 precipitation product based on the DPR dual-frequency algorithms. As a track-grade product, the GPM 2ADPR product has about 16 orbital data per day, which can intermittently provide users with precipitation information in the latitude range 65°S–65°N (Hou et al., 2014). According to the scan modes of the radar (Iguchi et al., 2012), the 2ADPR product can be subdivided into DPR_NS (KuPR normal scan), DPR_HS (KaPR high-sensitivity scan), and DPR_MS (KaPR matched scan) products. We used the

Table 1
The Onset Dates and End Dates of Meiyu Periods in Atypical Meiyu Years and Normal Meiyu Years, Based On the Historical Records of the Anhui Meteorological Observatory

Atypical year	Onset date	End date	Normal year	Onset date	End date
2005	5 July	29 July	2002	19 June	28 June
2008	14 June	23 June	2003	20 June	11 July
2011	9 June	25 June	2014	25 June	5 July
2015	24 June	24 July	2016	20 June	21 July
2018	19 June	11 July	2017	30 June	10 July

DPR_NS precipitation product, which contains Ku-band radar reflectivity profiles, rain rate profiles, rain types, and droplet size distribution profiles.

We used the geostationary observations from the Himawari-8 satellite, which was designed by the Japanese Meteorological Agency and has been operating at 140.7°E since July 2015. The Himawari-8 satellite carries the advanced Himawari Image with 16 different visible and infrared bands. We used the Himawari-8 data to obtain information on the cloud top and to identify the life stages of the precipitating clouds (Zhang & Fu, 2018).

ERA5 is the fifth-generation European Centre for Medium-Range Weather Forecasts (ECMWF) atmospheric reanalysis data set and covers the period from 1979 to 2 to 3 months before the present day (Hennermann & Berrisford, 2017). ERA5 has a time resolution of 1 hr and a horizontal resolution of about 31 km, which is much better than its predecessor (the ERA-Interim data set). We used environmental information from ERA5.

We also used the Integrated Global Radiosonde Archive (IGRA) data in this study. IGRA is a collection of historical and near-real-time radiosonde observations from around the globe. For most IGRA stations, the soundings are taken around 00:00 UTC and 12:00 UTC each day, providing the primary variables of temperature, humidity, and wind profiles. The soundings from Wuhan station, Fuyang station, Hangzhou station, and Anqin station were used in this study.

2.2. Methods

The study area covered the Yangtze Plain (28–34°N, 110–122°E; see Figure 3). Based on the historical records of the Anhui Meteorological Observatory, we focused on Meiyu periods of five atypical Meiyu years and five normal years in our study. The Meiyu periods in 2016 and 2018 were used as templates for selecting normal and atypical Meiyu periods, respectively. Three main criteria were employed including continuously cloudy or rainy day, sustained Meiyu fronts, and the intensity and location of subtropical high. The onset date and end date of each Meiyu period are given in Table 1.

The calculated water vapor flux of 850 hPa ($WV\text{flux}_{850}$; units: g/(m · Pa · s)) indicated low-level moisture transport:

$$WV\text{flux}_{850} = v_{850} q_{850} / g$$

where q_{850} (g/kg) is the specific humidity at 850 hPa, v_{850} (m/s) is the horizontal wind speed at 850 hPa, and g (m/s^2) is the gravitational acceleration.

3. Horizontal Distribution of Environmental Circulation and Precipitation

In any study of a weather event, it is essential to analyze the environmental flow field in which the event is located (Zhou et al., 2009). We therefore investigated the mean potential height, wind field, and specific humidity at 500 and 850 hPa during the Meiyu period in atypical Meiyu years (Figure 1). For comparison, Figure 2 shows the mean environmental circulation during the Meiyu period in normal Meiyu years.

During the East Asian summer, the 5,880-m contour lines in the 500-hPa geopotential height field reflect the location of the subtropical high, which is closely related to the Meiyu front (Zhu et al., 2008). During the atypical Meiyu periods, the area of subtropical high was small and located in southeast Japan (Figure 1a). The nearest distance of the subtropical high to the Yangtze Plain was about 10° of longitude, indicating that the

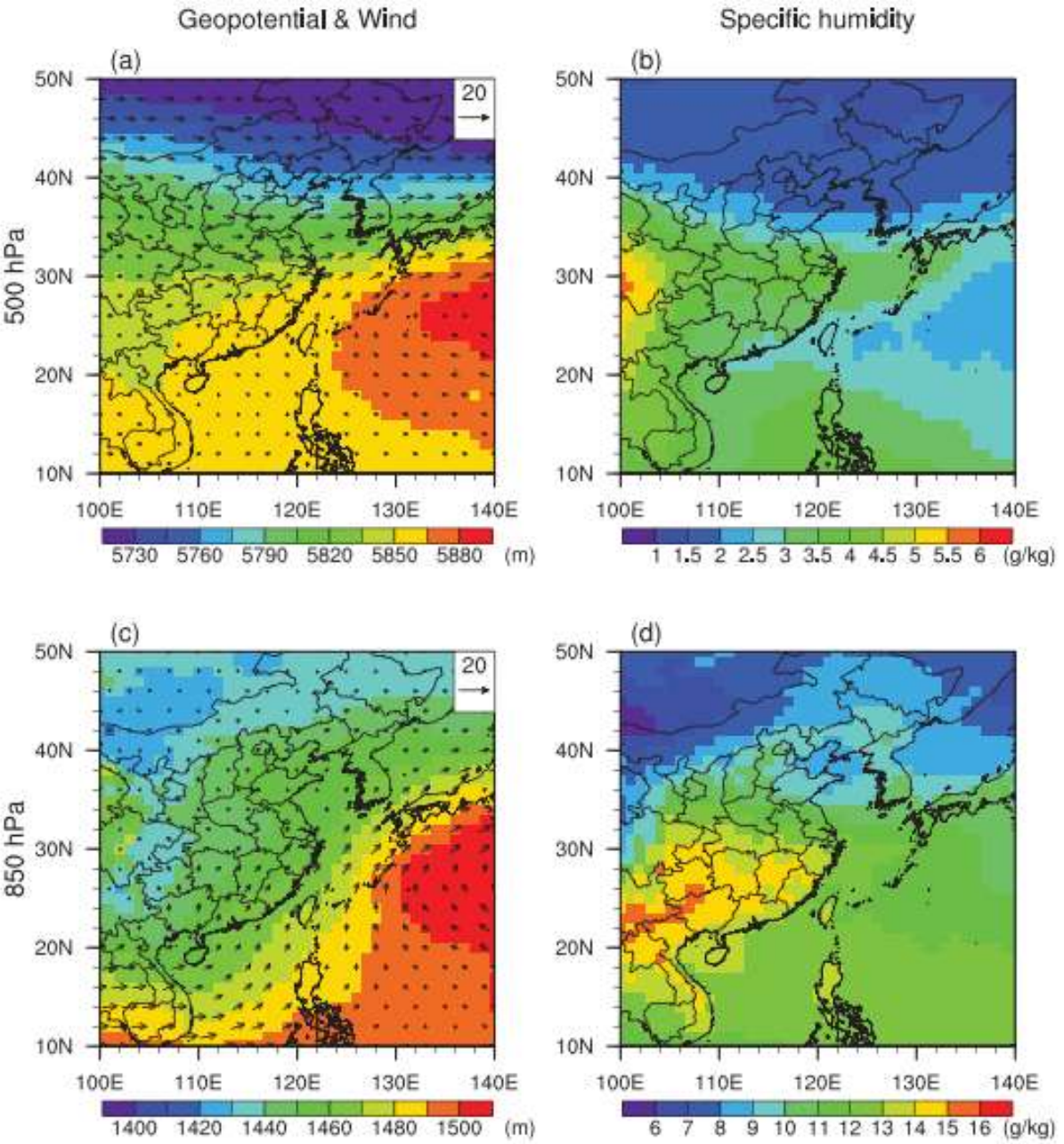

Figure 1. Distribution of (a) the 500-hPa geopotential height and wind, (b) the 500-hPa specific humidity, (c) the 850-hPa geopotential height and wind, and (d) the 850-hPa specific humidity during the Meiyu period in atypical Meiyu years.

impact of the subtropical high was weak. By contrast, the area of subtropical high during the normal Meiyu periods was much larger and located on the southeastern side of the Chinese mainland (Figure 2a). The location of the subtropical high was adjoined to the Yangtze Plain, indicating that the impact of subtropical high was strong. In addition, the average 500-hpa geopotential height in northern China during the atypical Meiyu periods was larger than that of normal periods (Figures 1a and 2a), indicating higher northern air pressure during the atypical Meiyu periods. The pressure gradient in the Yangtze Plain during the atypical Meiyu periods was affected by the subtropical high and the northern air pressure and was therefore much smaller than that in normal periods. As a result, the wind speed was lower and the Meiyu front was weaker. In addition, the stronger subtropical high during the normal Meiyu periods would provide

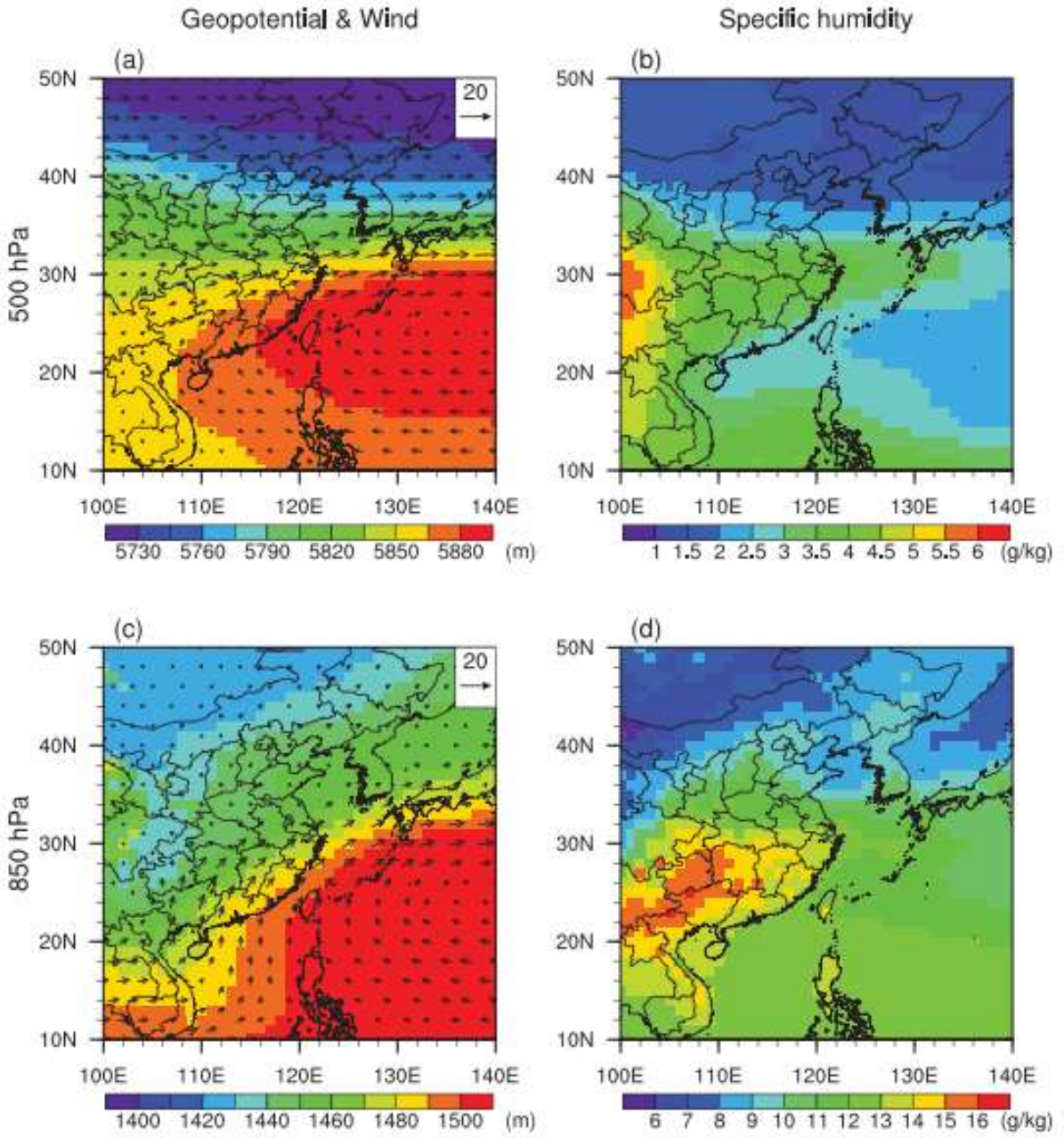

Figure 2. Distribution of (a) the 500-hPa geopotential height and wind, (b) the 500-hPa specific humidity, (c) the 850-hPa geopotential height and wind, and (d) the 850-hPa specific humidity during the Meiyu period in normal Meiyu years.

strong geotropic winds and warm conditions that promote wind diurnal amplitude in both dynamic and thermodynamic manners (Rao et al., 2019; Zeng et al., 2019). The enhanced wind diurnal amplitude during the normal Meiyu periods over the Yangtze Plain was thought to be beneficial for the morning rainfall peak (Xue et al., 2018).

The mean 850-hPa wind field was closely related to the location of the area of high pressure (Figures 1c and 2c). During the atypical Meiyu periods, the subtropical high was located to the east of the Yangtze Plain and the mean winds in the study area were southerly (Figure 1c). By contrast, during the normal Meiyu periods, the subtropical high was located on the southeast of the Yangtze Plain and the mean wind direction was

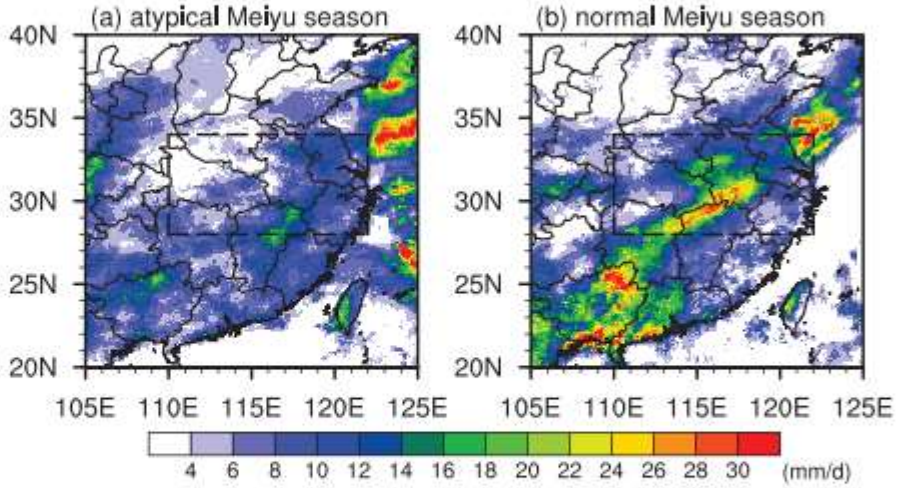

Figure 3. Distribution of the mean daily rainfall during the (a) atypical and (b) normal Meiyu periods in east China. The dashed rectangle indicates the location of the Yangtze Plain.

southwesterly with stronger wind speed (Figure 2c). The distribution of specific humidity shows that the main source of water vapor was in the southwest of Yangtze Plain (Figures 1b, 1d, 2b, and 2d), so the southwesterly wind during the normal Meiyu periods favored precipitation over the Yangtze Plain. Figures 1d and 2d show that the specific humidity of southwestern China was higher during the normal Meiyu periods, which was also beneficial to the precipitations in the downstream regions.

Figure 3 shows the mean daily precipitation in east China during the atypical and normal Meiyu periods. During the atypical Meiyu periods (Figure 3a), rainfall was scattered in east China and there was more rainfall in the Sichuan Basin, southern China, and the eastern ocean. In the study region, precipitation (10–20 mm/day) was mainly distributed south of the Yangtze River. During the normal Meiyu periods (Figure 3b), precipitation was concentrated in the Yangtze Plain and south China. There was a clear rainband extended from the southwest to the northeast of the study area with rainfall >25 mm/day. We suggest that this difference is related to the intensity and location of the subtropical high.

4. Morning Case

The horizontal distribution of environmental circulation and precipitation in atypical Meiyu periods were showed apparently different from that in normal Meiyu periods. In order to understand the causes, development, and structure of precipitation systems in atypical Meiyu periods, we present here two typical precipitation events captured by the GPM DPR during the IMFRE in 2018. The GPM satellite is a non-Sun-synchronous satellite, which transits the study area 1–2 times a day. The first case occurred at 10:20 LST (02:20 UTC) on 5 July 2018, and the relevant DPR characteristics are shown in Figure 4. It can be seen from the horizontal distribution (Figure 4a) that there were three main areas of precipitation in this precipitation event, labeled A (east of Hubei), B (north of Anhui), and C (northwest of Jiangsu) from west to east. The maximum rain rate at A and B was about 10 mm/hr, whereas the maximum rate of precipitation at C was >20 mm/hr. Both A and B showed mainly stratiform pixels, whereas there were numerous convective DPR pixels at C (Figure 4b).

Contoured frequency by altitude diagrams (CFADs) of radar echoes are a good indicator of the three-dimensional structural characteristics of clouds or precipitation events (Chen, Fu, et al., 2017). Figure 4c shows the CFAD distribution of the Ku-band echo for this precipitation event. The echo-top height of the Ku-band in this precipitation event was <10 km, and the echo reflectivity was <40 dBZ. As the precipitation event was dominated by stratiform precipitation, it can be seen that there was a distinct bright band at about 5.5 km as a result of the maximum reflectance of partially melted ice particles (Zhang et al., 2018). There is generally no bright band for convective precipitation because the melting layer is not uniform.

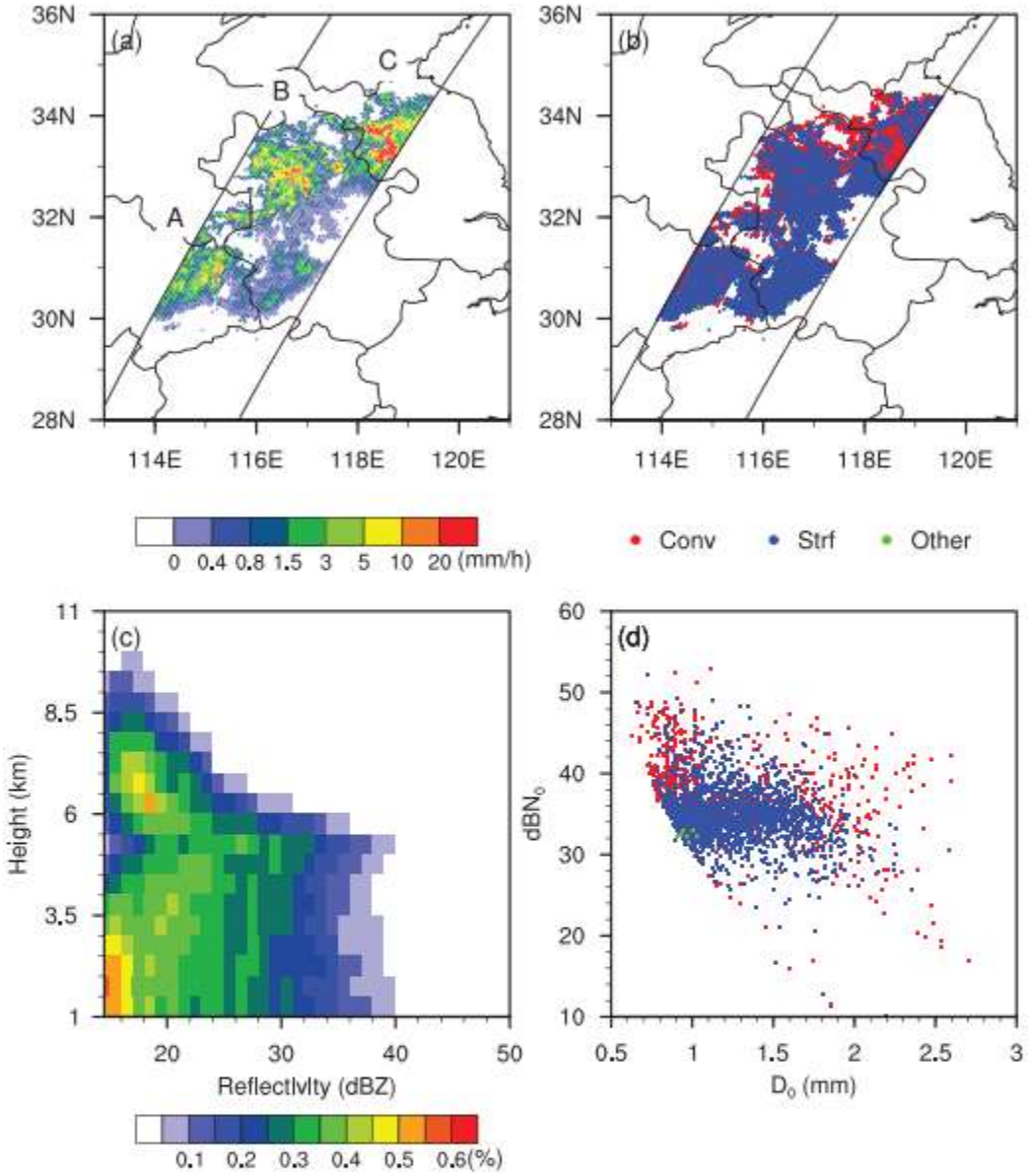

Figure 4. Horizontal distribution of (a) the near-surface rain rate, (b) the type of rain, (c) the CFAD of the Ku-band reflectivity, and (d) the scatter of near-surface droplets for the precipitation event at 10:20 LST on 5 July 2018. The labels A, B, and C indicate the three main areas of precipitation in this event from west to east.

Figure 4d shows the scattering of the near-surface droplet size distribution parameters retrieved by the dual-frequency algorithms, where dBN_0 represents the droplet concentration and D_0 is the effective droplet radius. The near-surface dBN_0 was about 30–38, whereas D_0 was around 0.9–1.8 for the stratiform precipitation in this event. The scattering of convective pixels can be divided into two types: One with a larger dBN_0 but smaller D_0 than the stratiform pixels and one with a larger D_0, corresponding to the shallow precipitation and nonshallow convective precipitation, respectively, in Wen et al. (2016). For this event, the shallow pixels occupied a larger proportion of the area and the maximum D_0 of the convective pixels was about 2.7 mm.

Figure 5 shows the distributions of the 500-hPa geopotential height and the 850-hPa water vapor flux in the East Asia within ±6 hr of the precipitation event. Although the intensity of the subtropical high (Figures 5a–5c) before and after the precipitation event was weaker than the mean of the 2018 Meiyu period (Figure 1a), the Yangtze Plain still presented a relatively stable westerly wind (Figures 5a–5c), indicating the existence of

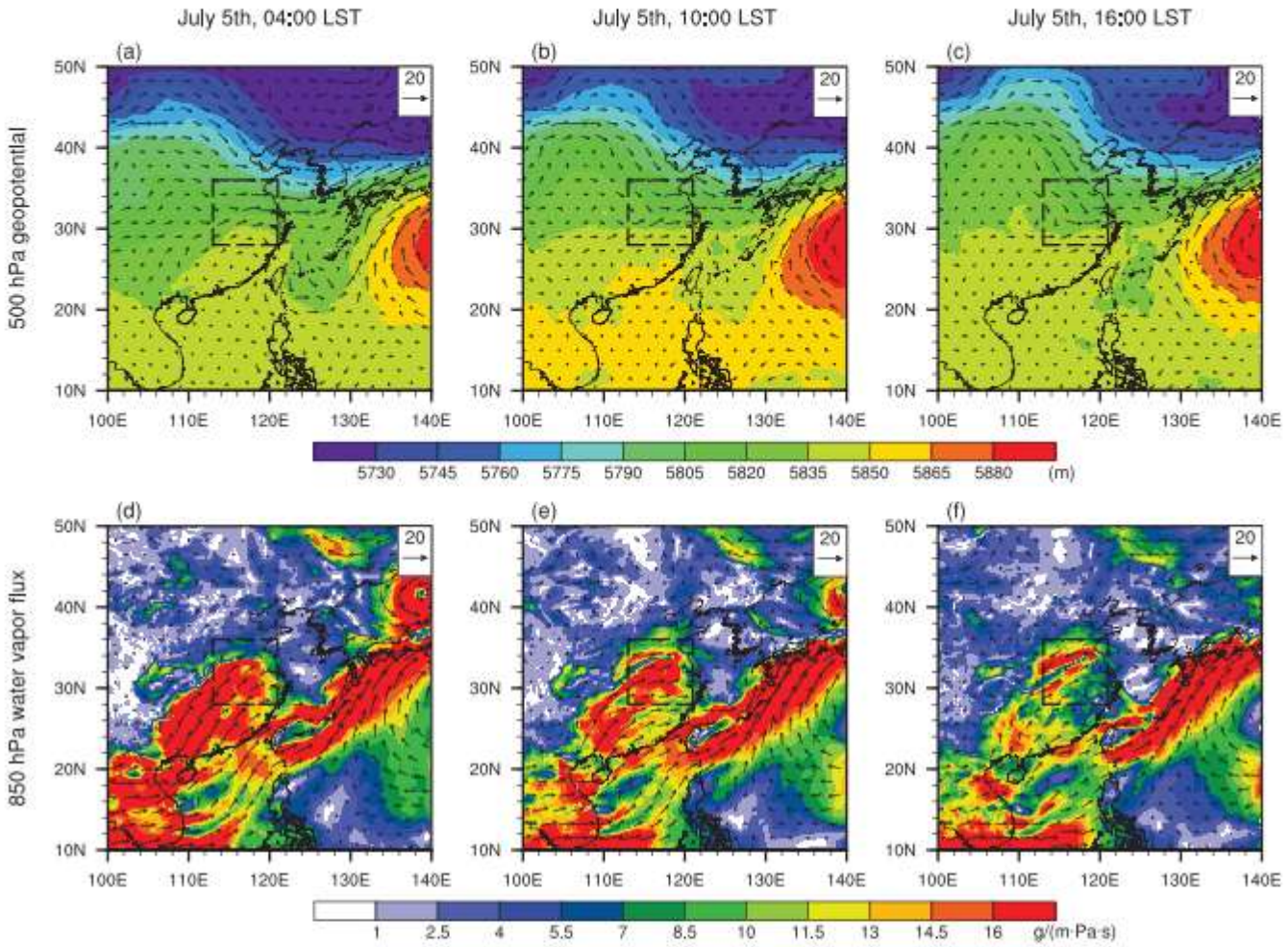

Figure 5. Horizontal distributions of (a–c) 500-hPa geopotential height and (d–f) 850-hPa water vapor flux within ±6 hr of the precipitation event that occurred at 10:20 LST on 5 July 2018. The dashed rectangle indicates the location of the precipitation event.

the Meiyu front. There was sufficient southwesterly water vapor flux at 850 hPa over the Yangtze Plain at and before the precipitation event (Figures 5d and 5e). The water vapor plume extended from southwest China to the east of the Yangtze Plain, with a water vapor flux of >16 g/(m·Pa·s) at 850 hPa. At the time of the precipitation event, there occurred a water vapor reflux from east to west on the north side of the water vapor plume (Figure 5e), which contributed to the low-level convergence of water vapor. At 16:00 LST, the southwesterly water vapor flux reduced to 7 g/(m·Pa·s; Figure 5f), while the water vapor reflux increased further in the area of precipitation.

Continuous monitoring of the cloud top brightness temperature can show the cloud evolution process over time (Zhang & Fu, 2018). Figure 6 shows the Himawari-8 10.4-μm brightness temperature within ±4 hr of the precipitation event. There were three cold clusters (A, B, and C) within the DPR orbit, at the time of the precipitation event (Figure 6e), which corresponds to the three regions of precipitation in Figure 4a. Among them, the minimum brightness temperature of cloud A was increasing and the area of cloud was decreasing, showing that cloud A was a typical dissipating cloud. We suggest that cloud A was formed by nocturnal strong southwesterly moisture transport and then dissipated as the moisture transport getting weaker during the day (Chen, Sha, et al., 2017; Xue et al., 2018). The precipitation corresponding to cloud A was therefore dominated by stratiform pixels with weak rain rates. During the dissipation process, much of the water vapor propagated along the water vapor plume and the new clouds B and C formed to the

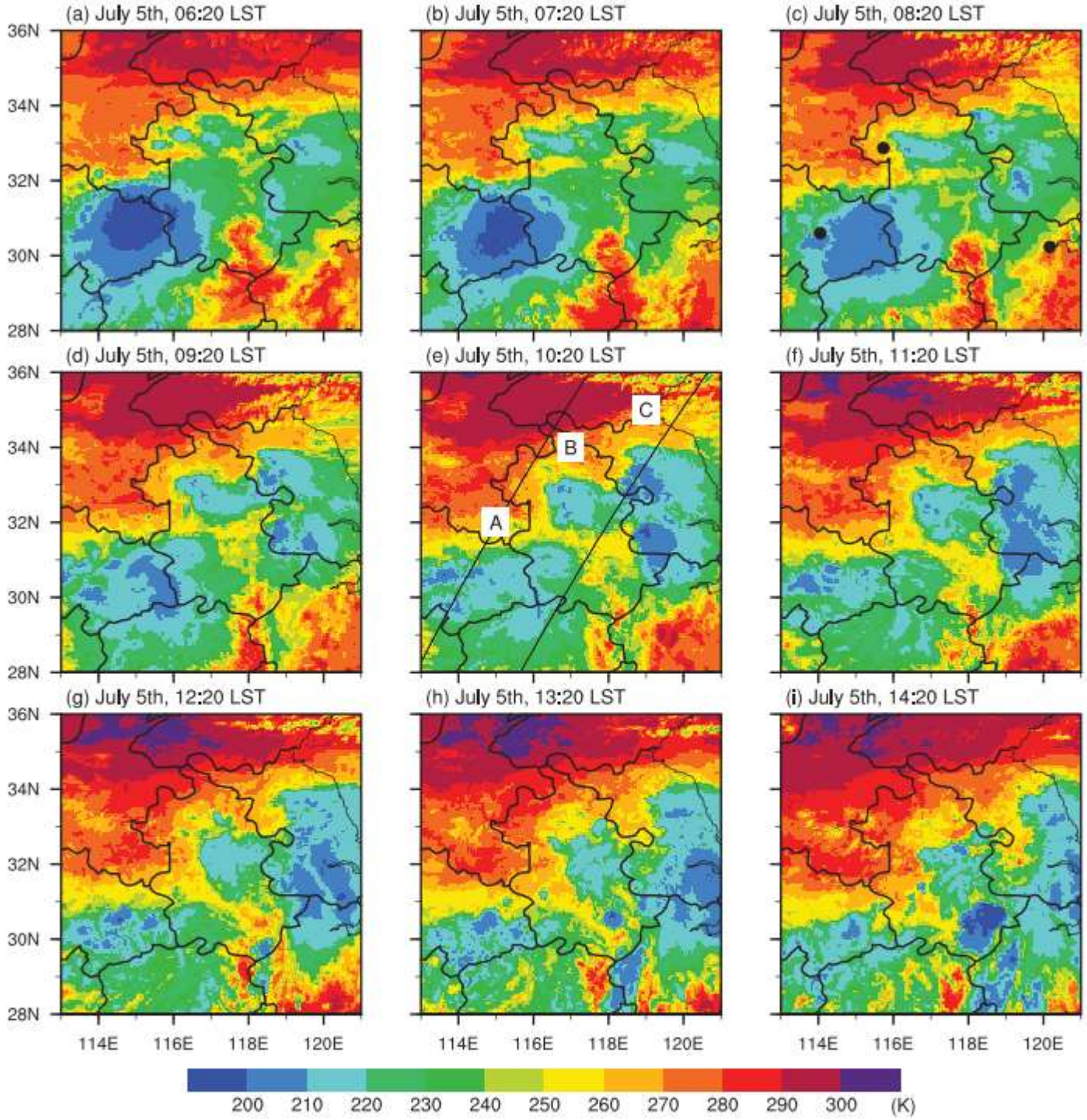

Figure 6. Horizontal distribution of the Himawari-8 10.4-μm brightness temperature before and after the occurrence of the precipitation event at 10:20 LST (02:20 UTC) on 5 July 2018. The diagonal lines represent the edges of the DPR swaths. The black dots in Figure 6c indicate the locations of Wuhan station, Fuyang station, and Hangzhou station (from left to right).

northeast of cloud A. At the position of cloud C, which was affected by low-level convergence (Figure 5e), the vertical updraft broke the morning inversion layer and there were therefore numerous convective pixels in the precipitating cloud C (Figure 4b).

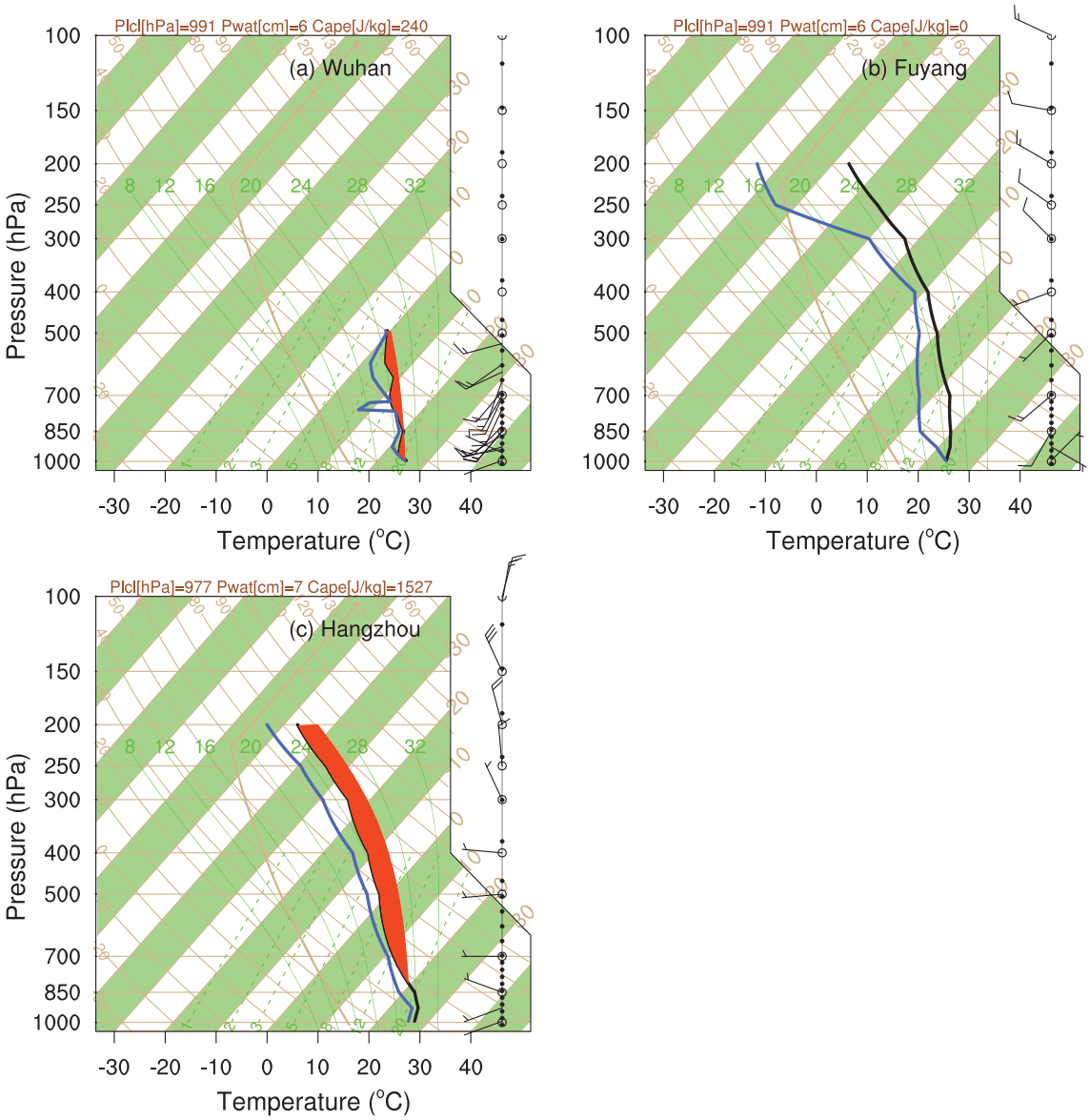

Figure 7. Radiosonde data in Skew-T-logP diagrams for (a) Wuhan station, (b) Fuyang station, and (c) Hangzhou station at 08:00 LST (00:00 UTC) on 5 July 2018. The black line and blue line indicate the profiles of temperature and dew point temperature, respectively. The red area in Figures 7a and 7b indicates the region of CAPE. The locations of the stations are shown in Figure 6c.

For a further knowledge of temperature and humidity features of the precipitating case, the IGRA sounding information ~2 hr before the precipitation case is given in Figure 7. The Wuhan station, Fuyang station, and Hangzhou station are located nearby the clouds A, B, and C, respectively. As shown in Figure 7, the pressure of Lifting Condensation Level was higher than 970 hPa for each station, and the temperature dew point difference was less than 7 °C below 300 hPa, showing that the middle- and low-level atmosphere was humid nearby the clouds. The Convective Available Potential Energy (CAPE) was ~0 for Wuhan and Fuyang station (Figures 7a and 7b), indicating that the atmospheric layer was quite stable and the convection was suppressed in clouds A and B. On the contrast, the CAPE of Hangzhou station reached 1,527 J/kg, indicating that the atmospheric layer in cloud C was unstable and beneficial to the convective activity, which was consistent with the above suggestions. The unstable layer appeared above 800 hPa, indicating that the convection is a kind of elevated convection.

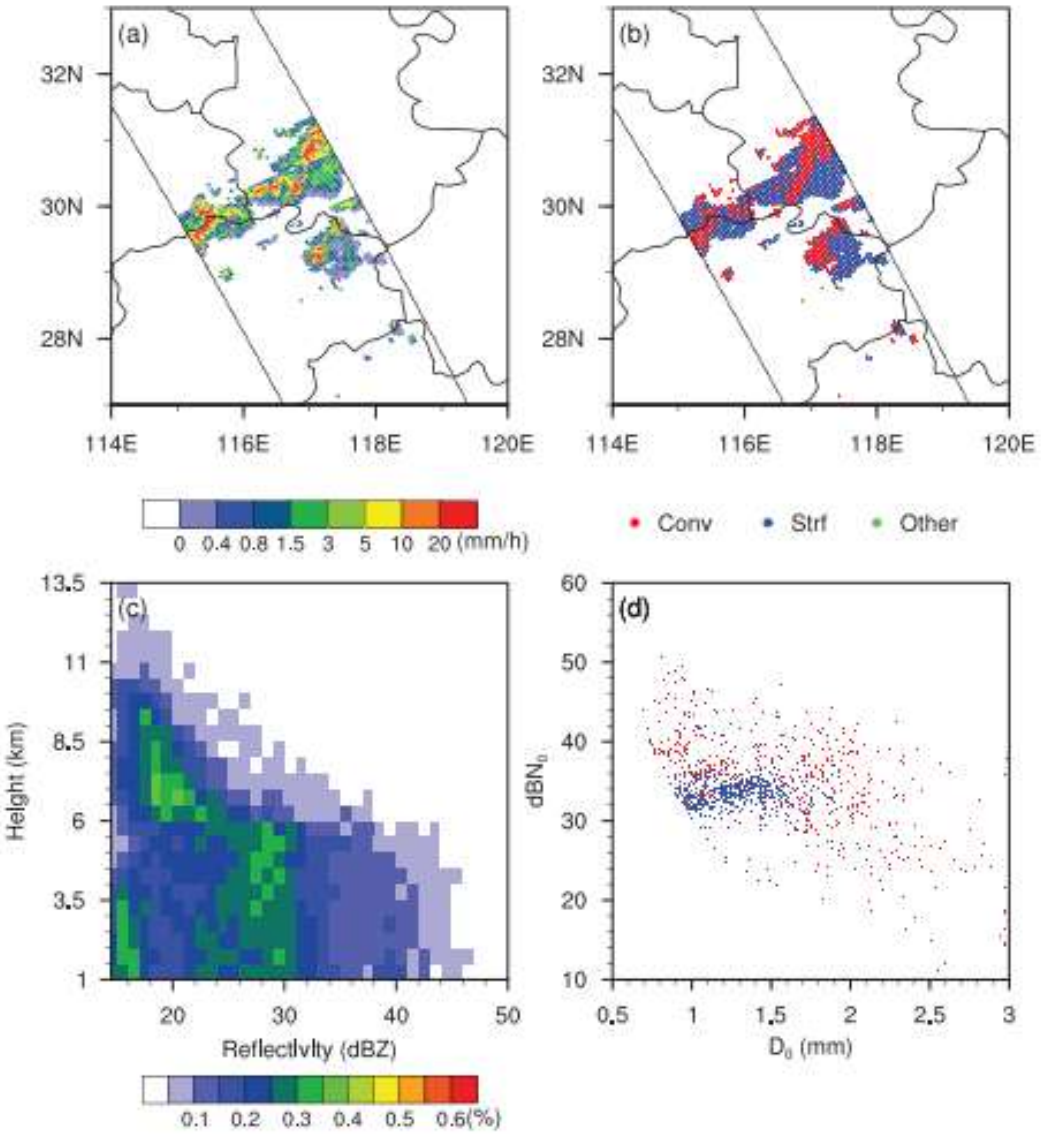

Figure 8. Horizontal distribution of (a) the near-surface rain rate, (b) the type of rain, (c) the CFAD of the Ku-band reflectivity, and (d) the scatter of near-surface droplets for the precipitation event at 20:04 LST on 5 July 2018.

5. Evening Case

The evening case occurred at 20:04 LST (12:04 UTC) on 5 July 2018, 10 hr after the previous event. The precipitation event was located at the junction of Hubei, Anhui, and Jiangxi provinces in the southern region of the Yangtze Plain (Figure 8a). The precipitation event consisted of several small rain cells with rough boundaries, and the instantaneous rain rate was >20 mm/hr. There was a large proportion of convective pixels in this event (Figure 8b), indicating that it was a typical convective event. The echo-top height for this event was >13.5 km, with a maximum echo reflectivity >45 dBZ, and there was no obvious bright band in the CFAD contours (Figure 8c). The maximum near-surface D_0 was >3 mm (Figure 8d), much larger than in the first event (Figure 4d), which may be related to the stronger updraft within this second event (Hocking, 1959).

The distributions of the environmental circulation and Himawari-8 brightness temperature before and after the precipitation event are shown in Figures 9 and 10, respectively. Low-level convergence began to appear

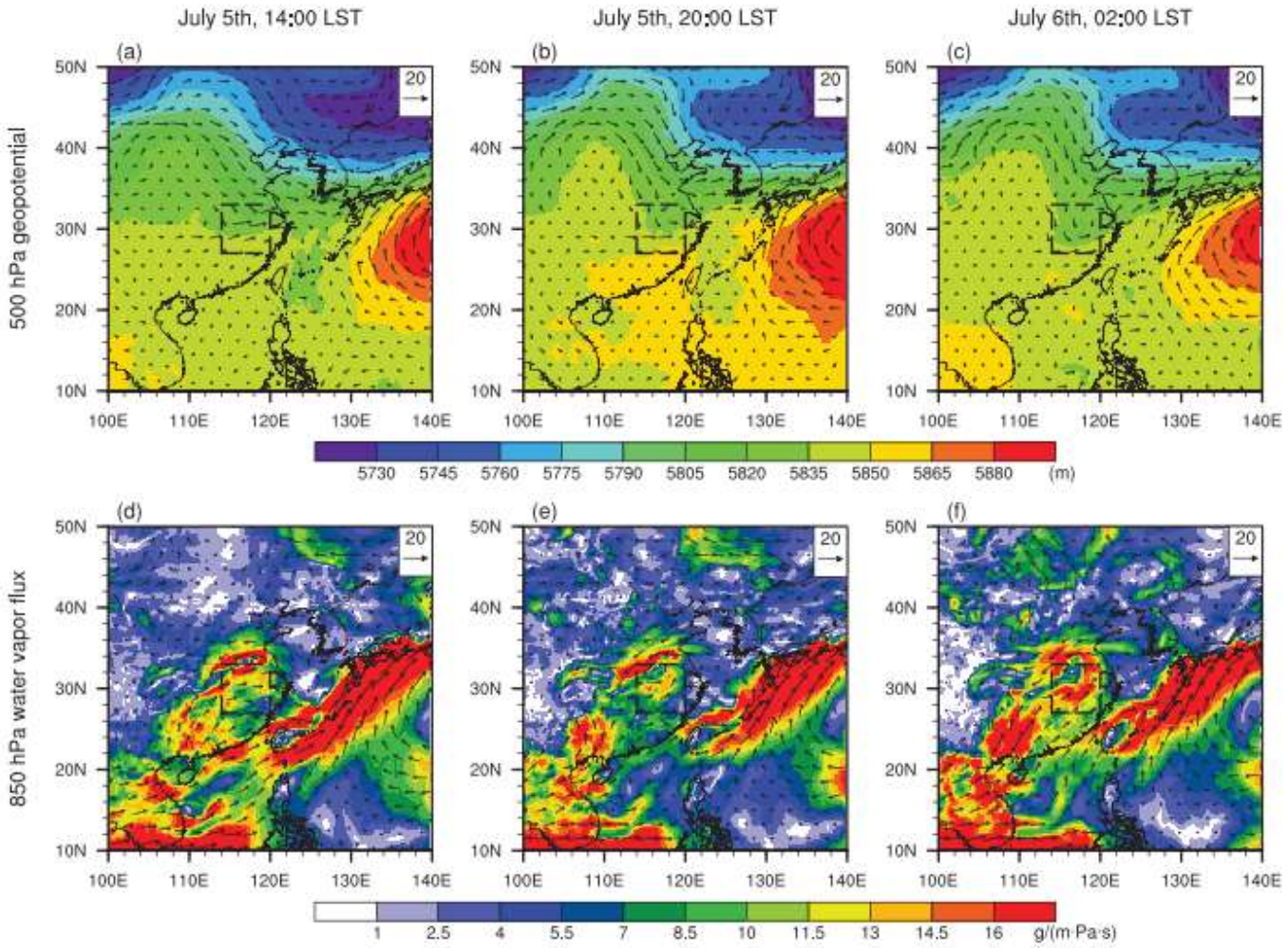

Figure 9. Horizontal distributions of (a–c) 500-hPa geopotential height and (d–f) 850-hPa water vapor flux within ±6 hr of the precipitation event that occurred at 20:04 LST on 5 July 2018. The dashed rectangle indicates the location of the precipitation event.

in the Yangtze Plain at 10:00 LST (Figure 5e). This low-level convergence increased over time (Figures 9d–9f) and gradually developed up to the 500-hPa pressure level (Figures 9a–9c). At the time of precipitation, the westerly winds in the Yangtze Plain became cyclonic at 500 hPa, which marked the transformation of the Meiyu front to a Jianghuai cyclone. The convective precipitation event occurred to the southeastern of the extratropical cyclone, a warm zone surrounded by two cyclonic fronts (Bjerknes, 1919). The precipitating cloud developed and enhanced as the Jianghuai cyclone gradually formed (Figure 10). The inner updraft was very strong at this time, preventing small raindrops from falling, and the near-surface droplets were large (Figure 8d).

The sounding information for this case is shown in Figure 11, which is taken just 4 min before the DPR swath. Clearly, it is shown that the temperature dew point difference was less than 1 °C below 400 hPa and the CAPE reached 2,617 J/kg, indicating that the atmospheric environment within the precipitating case was very moist and unstable, consistent with large amount of intensive convective precipitating pixels detected by DPR (Figure 8). Moreover, there existed obvious wind shear in the atmospheric layer (Figure 11). The low-level winds were southwesterly, while the high-level winds were northerly, showing the presence of baroclinic atmospheric system, which we suggested above to be the initiation of Jianghuai cyclone.

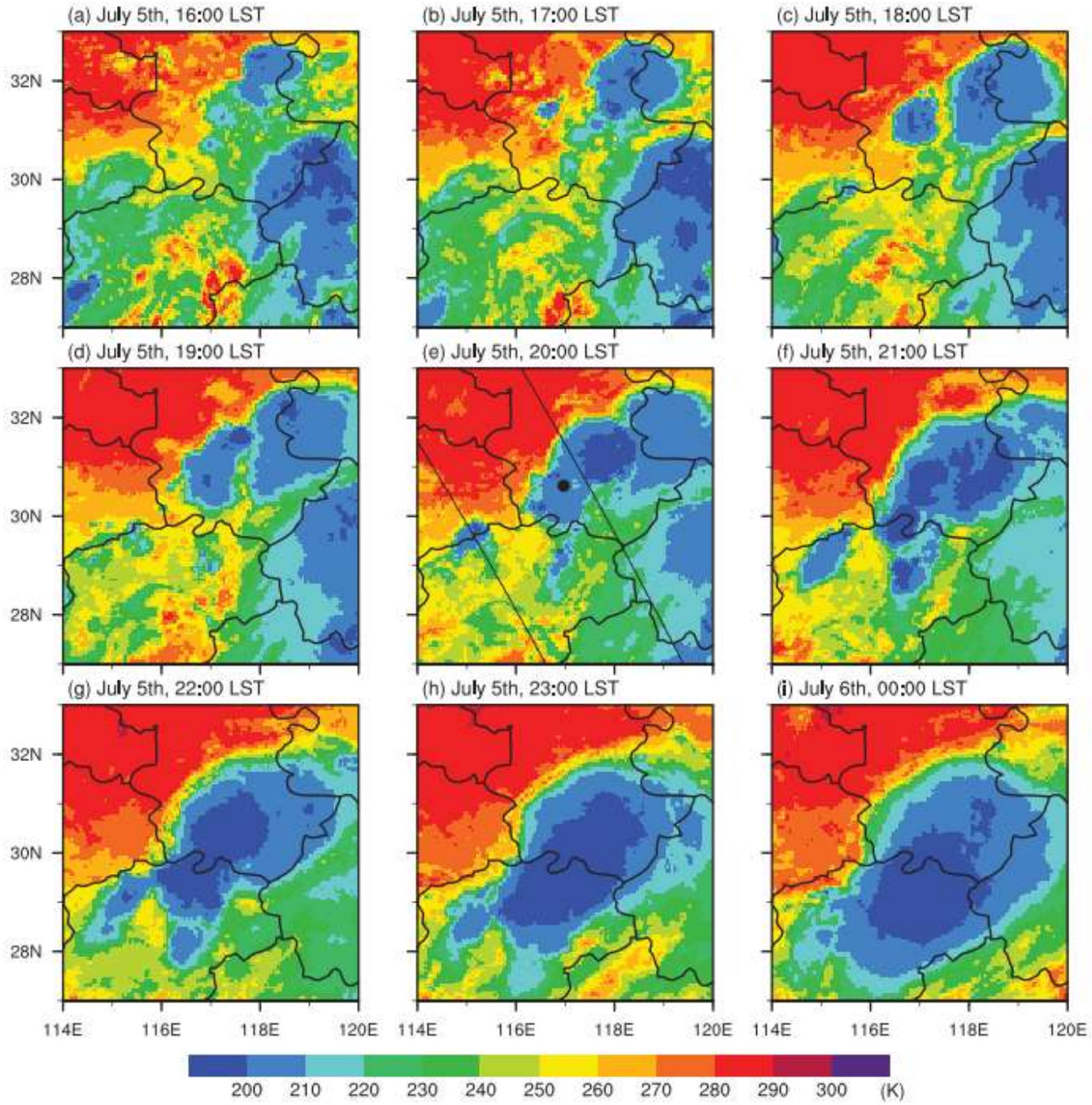

Figure 10. Horizontal distribution of the Himawari-8 10.4-μm brightness temperature before and after the occurrence of the precipitation event at 20:04 LST on 5 July 2018. The diagonal lines represent the edges of the DPR swath. The black dot indicates the location of Anqin station.

6. Diurnal Variation of Meiyu Rainfall

This section specifically focuses on the diurnal variation in Meiyu precipitation during the atypical and normal Meiyu periods and explores the possible causes for this by considering previously reported case studies and hereafter statistical researches of the environmental information.

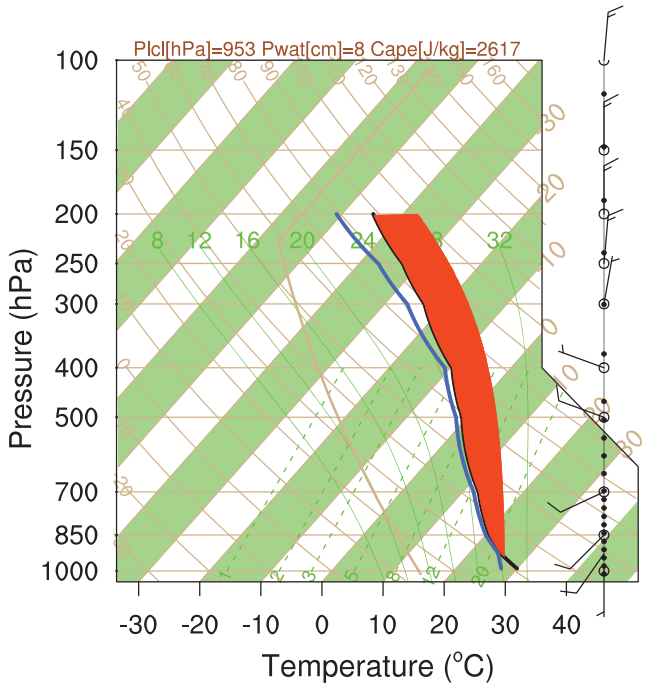

Figure 11. Radiosonde data in Skew-T-logP diagram for Anqin station at 20:00 LST (12:00 UTC) on 5 July 2018. The black line and blue line indicate the profiles of temperature and dew point temperature, respectively. The red area indicates the region of CAPE. The location of Anqin station is shown in Figure 10e.

Previous research on the diurnal variation in precipitation on the Yangtze Plain has shown that in summer, the diurnal variation of precipitation in the Yangtze Plain appears as a double peak in the early morning (at about 06:00 LST) and late afternoon (at about 17:00 LST; Yu, Zhou, et al., 2007). The early morning peak was previously thought to be the only peak in the diurnal cycle of precipitation during the Meiyu period (Geng & Yamada, 2007; Xue et al., 2018). We compared the patterns of diurnal variation in Meiyu rainfall with the atypical Meiyu years (like 2018) and the normal Meiyu years (like 2016; Figure 12).

Using GPM IMERG data of five atypical Meiyu periods and five normal Meiyu periods (listed in Table 1), we carried out statistical studies on the diurnal variations of Meiyu rainfall over the Yangtze Plain. During the atypical Meiyu periods, the mean precipitation over the Yangtze Plain ranged from 0.3 to 0.45 mm/hr (Figure 12). The diurnal variation in the rain rate appeared as a bimodal structure, with peaks in the early morning (6:30 LST) and afternoon (16:00 LST). The bimodal structure was similar to that seen in summer (Yu, Zhou, et al., 2007; Yu, Xu, et al., 2007), although the afternoon peak occurred 1 hr earlier.

During the normal Meiyu periods, the mean precipitation ranged from 0.4 to 0.65 mm/hr (Figure 12). The diurnal variation appeared as a single distribution with the peak time at ~09:30 LST. The diurnal variation of rainfall in the normal Meiyu periods was similar to the Previous study except that the peak time was 1.5 hr later (Geng & Yamada, 2007). The diurnal variances of atypical Meiyu years and normal Meiyu years verified that the diurnal cycle of Meiyu rainfall varies from year to year.

Figure 13 shows the mean distribution of the 500-hPa geopotential height and wind in East Asia at different local times during the Meiyu period. The subtropical high was weak during the atypical Meiyu periods and was located 10° of longitude to the east of the Yangtze Plain (Figures 13a–13c). The contour lines in the Yangtze Plain were sparse, and the mean winds were weak. On the contrast, the subtropical high was strong during the normal Meiyu periods and located close to the southeast of the Yangtze Plain (Figures 13d–13f). The 500-hPa contour lines in the study area were dense with strong winds. From the perspective of the diurnal variation, the geopotential height decreased during the daytime as a result of solar heating (Figures 13c and 13f), whereas the geopotential heights increased during the nighttime due to atmospheric cooling (Figures 13a and 13d). The enhanced subtropical high during the nighttime would provide stronger geotropic winds and warmer conditions that is beneficial for the occurring of morning precipitations (Rao et al., 2019; Zeng et al., 2019).

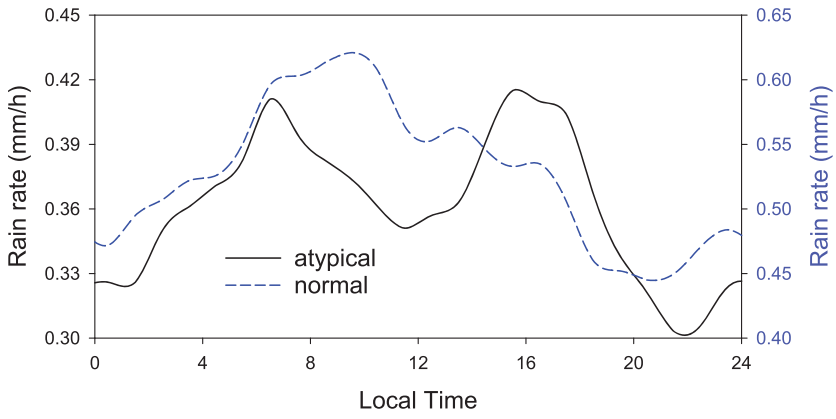

Figure 12. Diurnal variation in mean precipitations averaged over the Yangtze Plain during the Meiyu periods in atypical Meiyu years (left) and normal Meiyu years (right), derived from GPM IMERG products.

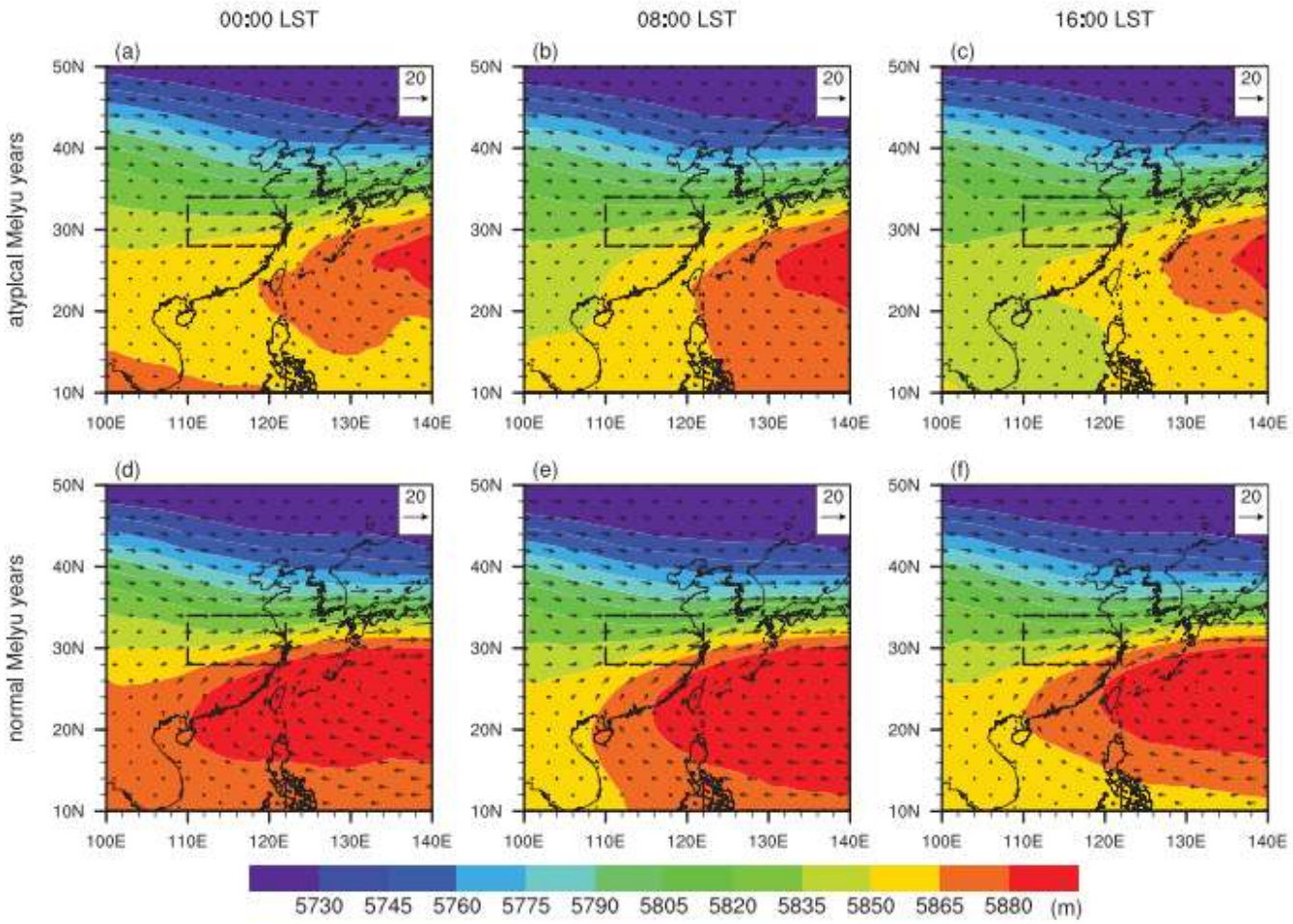

Figure 13. Average distribution of the 500-hPa geopotential height and wind at different local times during the Meiyu periods in (a–c) atypical Meiyu years and (d–f) normal Meiyu years.

Figure 14 shows the mean 850-hPa water vapor flux at different local times. The water vapor flux in the Yangtze Plain showed a significant diurnal variation during Meiyu periods as a result of the diurnal rotation of the ageostrophic winds in the south of the study region (Xue et al., 2018). In the midnight and morning, the direction of the ageostrophic winds was similar to that of the geotropic winds, so the total wind speed was very high and there was a high calculated water vapor flux (Figures 14a, 14b, 14d, and 14e). By contrast, the total wind speed was low in the late afternoon (Figures 14c and 14f) due to the obtuse angle between the ageostrophic and geotropic winds and hence the water vapor flux was weak. Triggered by the southwesterly strong moisture transport, the morning precipitations were mainly composed of stratiform precipitations (not shown).

The afternoon rainfall maxima have often been reported over continent regions (e.g., Garreaud & Wallace, 1997; Yang & Smith, 2006). The most popular explanations for the afternoon peak are various manifestations of the land surface heating mechanism (Pielke, 2013; Yang & Smith, 2006). The diurnally modulated land surface heating affects the static destabilization of the atmosphere both within the planetary boundary layer (PBL) and the free troposphere. The dry and moist static stability variations lead to the growth of dry and moist convective overturning. Thunderstorms generally arise from deep convective overturning, which will not take place until the dry convective overturning process penetrates the PBL. Since the static stability usually reaches its lower point in the afternoon, the dry convective overturning process would be more likely to penetrate the PBL at this time, and the afternoon showers often appear with the deep convective

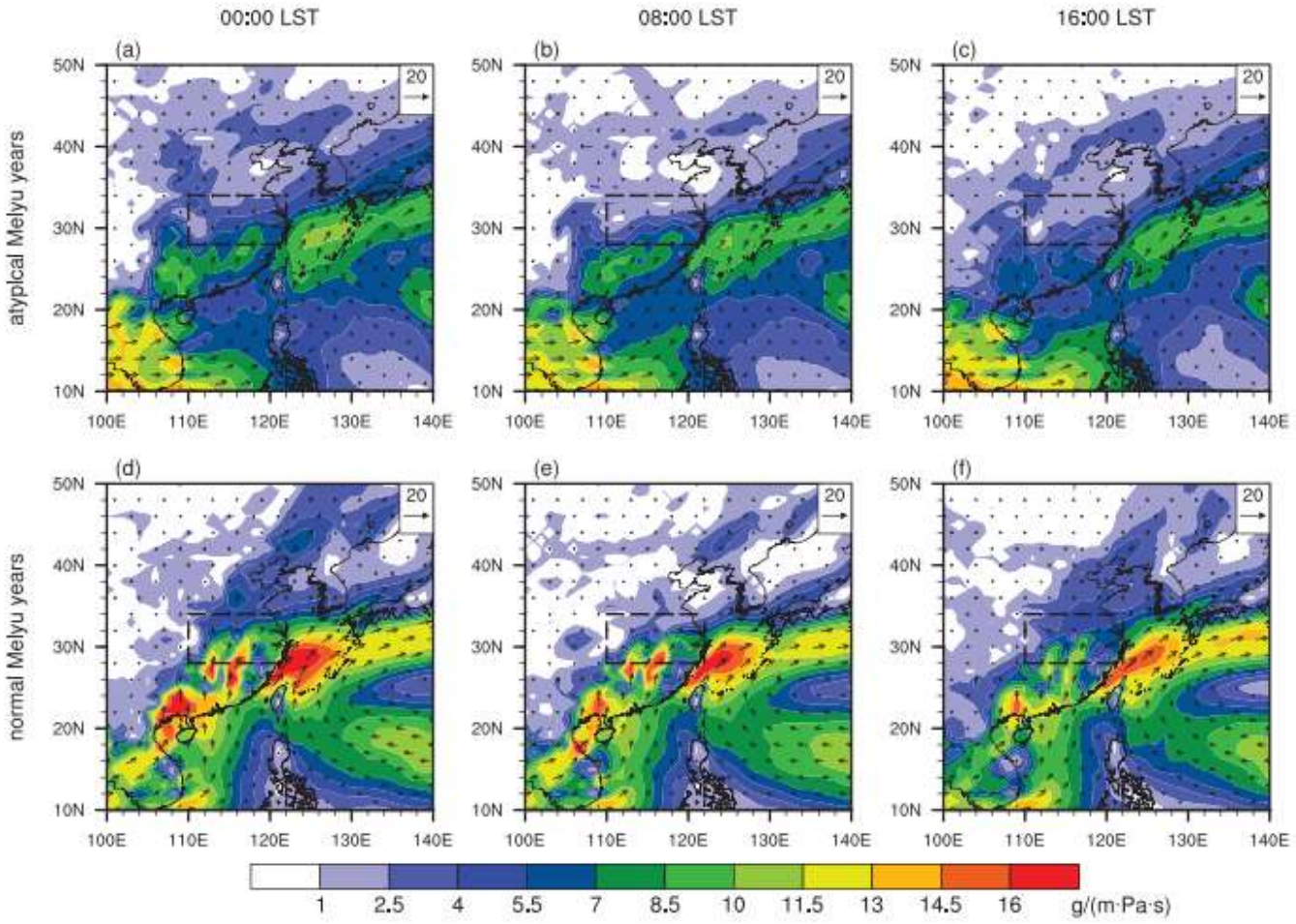

Figure 14. Average distribution of the 850-hPa water vapor flux at different local times during the Meiyu periods in atypical Meiyu years and (d–f) normal Meiyu years.

overturning process. In such condition, a large proportion of convective pixels was found within the afternoon precipitations during the Meiyu periods over the Yangtze Plain (not shown).

In addition, there were some suggestions that there existed no afternoon precipitation peak in normal Meiyu periods but existed in atypical Meiyu periods. During the normal Meiyu periods, there is sustained cloudiness along the active Meiyu front, which may reduce solar radiation in the following daytime and thus resulting in the suppressed afternoon convection. And it is just the opposite for normal Meiyu periods.

7. Discussion and Conclusions

In an attempt to reveal the diurnal variations of Meiyu rainfall over the Yangtze Plain in the atypical Meiyu years, we analyzed two typical precipitation events during the 2018 (an atypical Meiyu year) IMFRE in detail, one in the morning and one in the afternoon. We then compared the diurnal variations in the atypical Meiyu precipitation with the normal Meiyu periods using statistics from GPM IMERG and ERA5 and explored the possible triggers. Our main conclusions are as follows.

The overall environmental circulation and precipitation over East Asia were studied during the atypical and normal Meiyu periods. During the atypical Meiyu periods, the subtropical high was weak and located 10° of longitude to the east of the Yangtze Plain. The geopotential contour lines in the Yangtze Plain were sparse, and the mean winds were weak. By contrast, during the normal Meiyu periods, the subtropical high was strong and located in the southeast of the Yangtze Plain. The geopotential contour lines in the study area

were dense with strong winds. Precipitation during the atypical Meiyu periods was sparsely distributed in the Sichuan Basin, southern China, and the eastern ocean, where the precipitation in normal Meiyu periods was concentrated on the Yangtze Plain, forming a clear southwest-northeast rain belt.

We conducted case studies of two heavy precipitation events detected by the GPM DPR during the IMFRE in 2018. These two events occurred at 10:20 and 20:04 LST on 5 July 2018. The morning event was divided into three rain cells (A–C) along the water vapor plume from the southwest to the northeast of the Yangtze Plain. Among these, rain cell A consisted of typical stratiform precipitation induced by strong southwesterly moisture transport. The corresponding cloud cluster of rain cell A dissipated as a result of daytime solar heating. During the dissipation process, a large amount of water vapor propagated along the water vapor plume and new precipitating clouds B and C formed to the northeast of cloud A. There were numerous convective DPR pixels in precipitating cloud C, which was affected by low-level convergence.

The late afternoon event occurring in the south of the Yangtze Plain was a typical convective precipitating event. At that time, the Meiyu front was changing into the Jianghuai cyclone and the precipitation was located in the southeast of the cyclone. The corresponding cloud system was in the process of developing and enhancing within the strong inner updraft. As a result of the strong convection, the Ku-band echo-top was >13.5 km and the maximum near-surface effective droplet radius was >3 mm. These two case studies indicate that heavy precipitation in the morning during Meiyu period relies heavily on the low-level moisture supply, whereas precipitation in the afternoon is affected by updrafts.

Previous studies have shown that a single morning peak dominates the diurnal cycle of Meiyu rainfall in the Yangtze Plain (Geng & Yamada, 2007; Xue et al., 2018). However, our results suggest that in the atypical Meiyu periods, the diurnal variation of precipitation had a bimodal structure, with peaks in early morning (6:30 LST) and afternoon (16:00 LST). In the normal Meiyu years, the diurnal variation of precipitation peaks in the morning at ~09:30 LST. We think that the morning peak of Meiyu precipitations is related to the diurnal variation of the low-level moisture supply. During the Meiyu period, the water vapor flux in the Yangtze Plain was characterized by a strong morning flux and a weak afternoon flux. The afternoon peak in the atypical Meiyu periods is related to the daytime local solar heating, while the low-level horizontal flow is thought to be unfavorable.

Our research suggests that the diurnal variation in Meiyu rainfall over the Yangtze Plain changes from year to year. However, more evidence is required and the causes should be investigated in detail. Future studies should pay attention to the correlation between the diurnal cycle of Meiyu rainfall and environmental factors, such as the subtropical high, the El Niño–Southern Oscillation, and the East Asian monsoon, which could provide powerful references for simulating and predicting Meiyu precipitation.

Acknowledgments
This research was supported by the National Key R&D Program of China under Grant 2017YFC1501402 and 2018YFC1507200, NSFC Project under Grant 41620104009, 41675041, and 91837310, and the Key research and development projects in Anhui province under Grant 201904a07020099. The IMERG and 2ADPR precipitation data used in this study were collected from the Precipitation Measurement Mission website (https://pmm.nasa.gov). The ERA5 reanalysis data used in this study were collected form the ECMWF website (https://apps.ecmwf.int/). We would also like to acknowledge the Japanese Meteorological Agency for providing the Himawari-8 data (http://www.data.jma.go.jp/mscweb/en/himawari89/) and the National Oceanic and Atmospheric Administration (NOAA) for providing IGRA sounding data (www.ncdc.noaa.gov).

References

Asai, T., Ke, S., & Kodama, Y. M. (1998). Diurnal variability of cloudiness over East Asia and the Western Pacific Ocean as revealed by GMS during the warm season. *Journal of the Meteorological Society of Japan*, *76*(5), 675–684. https://doi.org/10.2151/jmsj1965.76.5_675

Bjerknes, J. (1919). On the structure of moving cyclones. *Monthly Weather Review*, *47*(2), 95–99. https://doi.org/10.1175/1520-0493(1919)47<95:OTSOMC>2.0.CO;2

Chang, C. P., Zhang, Y., & Li, T. (2000). Interannual and interdecadal variations of the east Asian summer monsoon and tropical Pacific SSTs. Part I: Roles of the subtropical ridge. *Journal of Climate*, *13*(24), 4310–4325. https://doi.org/10.1175/1520-0442(2000)013<4310:IAIVOT>2.0.CO;2

Chen, G., Sha, W., & Iwasaki, T. (2009a). Diurnal variation of precipitation over southeastern China: Spatial distribution and its seasonality. *Journal of Geophysical Research*, *114*, D13103. https://doi.org/10.1029/2008JD011103

Chen, G., Sha, W., & Iwasaki, T. (2009b). Diurnal variation of precipitation over southeastern China: 2. Impact of the diurnal monsoon variability. *Journal of Geophysical Research*, *114*, D21105. https://doi.org/10.1029/2009JD012181

Chen, G., Sha, W., Iwasaki, T., & Ueno, K. (2012). Diurnal variation of rainfall in the Yangtze River Valley during the spring-summer transition from TRMM measurements. *Journal of Geophysical Research*, *117*, D06106. https://doi.org/10.1029/2011JD017056

Chen, G., Sha, W., Iwasaki, T., & Wen, Z. (2017). Diurnal cycle of a heavy rainfall corridor over East Asia. *Monthly Weather Review*, *145*(8), 3365–3389. https://doi.org/10.1175/MWR-D-16-0423.1

Chen, G., Yoshida, R., Sha, W., Iwasaki, T., & Qin, H. (2014). Convective instability associated with the eastward-propagating rainfall episodes over eastern China during the warm season. *Journal of Climate*, *27*(6), 2331–2339. https://doi.org/10.1175/JCLI-D-13-00443.1

Chen, Y., Fu, Y., Xian, T., & Pan, X. (2017). Characteristics of cloud cluster over the steep southern slopes of the Himalayas observed by CloudSat. *International Journal of Climatology*, *37*(11), 4043–4052. https://doi.org/10.1002/joc.4992

Ding, Y. H. (1992). Summer monsoon rainfalls in China. *Journal of the Meteorological Society of Japan*, *70*(1B), 373–396. https://doi.org/10.2151/jmsj1965.70.1B_373

Garreaud, R. E. D., & Wallace, J. M. (1997). The diurnal march of convective cloudiness over the Americas. *Monthly Weather Review*, *125*(12), 3157–3171. https://doi.org/10.1175/1520-0493(1997)1252.0.CO;2

Ge, Q., Guo, X. F., Zheng, J. Y., & Hao, Z. X. (2008). Meiyu in the middle and lower reaches of the Yangtze River since 1736. *Chinese Science Bulletin*, *53*(1), 107–114. https://doi.org/10.1007/s11434-007-0440-5

Geng, B., & Yamada, H. (2007). Diurnal variations of the Meiyu/Baiu rain belt. *Sola*, *3*, 61–64. https://doi.org/10.2151/sola.2007-016

Hennermann, K., & Berrisford, P. (2017). ERA5 data documentation, *Copernicus knowledge base*.

Hocking, L. M. (1959). The collision efficiency of small drops. *Quarterly Journal of the Royal Meteorological Society*, *85*(363), 44–50. https://doi.org/10.1002/qj.49708536305

Hou, A. Y., Kakar, R. K., Neeck, S., Azarbarzin, A. A., Kummerow, C. D., Kojima, M., et al. (2014). The Global Precipitation Measurement mission. *Bulletin of the American Meteorological Society*, *95*(5), 701–722. https://doi.org/10.1175/bams-d-13-00164.1

Iguchi, T., Seto, S., Meneghini, R., Yoshida, N., Awaka, J., Kubota, T., et al. (2012). An overview of the precipitation retrieval algorithm for the Dual-frequency Precipitation Radar (DPR) on the Global Precipitation Measurement (GPM) mission's core satellite. *Earth Observing Missions and Sensors: Development, Implementation, and Characterization II, International Society for Optics and Photonics*, *8528*, 85281C. https://doi.org/10.1117/12.977352

Li, H., He, S., Fan, K., & Wang, H. (2019). Relationship between the onset date of the Meiyu and the South Asian anticyclone in April and the related mechanisms. *Climate Dynamics*, *52*(1-2), 209–226. https://doi.org/10.1007/s00382-018-4131-5

Li, W., Luo, C., Wang, D., & Lei, T. (2010). Diurnal variations of precipitation over the South China Sea. *Meteorology and Atmospheric Physics*, *109*(1-2), 33–46. https://doi.org/10.1007/s00703-010-0094-8

Luo, J., Tian, W., Pu, Z., Zhang, P., Shang, L., Zhang, M., & Hu, J. (2013). Characteristics of stratosphere-troposphere exchange during the Meiyu season. *Journal of Geophysical Research: Atmospheres*, *118*, 2058–2072. https://doi.org/10.1029/2012JD018124

Nesbitt, S. W., & Zipser, E. J. (2003). The diurnal cycle of rainfall and convective intensity according to three years of TRMM measurements. *Journal of Climate*, *16*(10), 1456–1475. https://doi.org/10.1175/1520-0442(2003)016<1456:tdcora>2.0.co;2

Ninomiya, K., & Akiyama, T. (1992). Multiscale features of Baiu, the summer monsoon over Japan and the east-Asia. *Journal of the Meteorological Society of Japan*, *70*(1B), 467–495. https://doi.org/10.2151/jmsj1965.70.1B_467

Ninomiya, K., & Shibagaki, Y. (2007). Multi-scale features of the Meiyu-Baiu front and associated precipitation systems. *Journal of the Meteorological Society of Japan*, *85B*, 103–122. https://doi.org/10.2151/jmsj.85B.103

Pielke, R. A. (2013). *Mesoscale meteorological modeling*. Cambridge: Academic Press.

Rao, X., Zhao, K., Chen, X., Huang, A., Xue, M., Zhang, Q., & Wang, M. (2019). Influence of synoptic pattern and low-level wind speed on intensity and diurnal variations of orographic convection in summer over Pearl River Delta, South China. *Journal of Geophysical Research: Atmospheres*, *124*, 6157–6179. https://doi.org/10.1029/2019JD030384

Sampe, T., & Xie, S. (2010). Large-scale dynamics of the Meiyu-Baiu rainband: Environmental forcing by the westerly jet*. *Journal of Climate*, *23*(1), 113–134. https://doi.org/10.1175/2009JCLI3128.1

Sun, X., Greatbatch, R. J., Park, W., & Latif, M. (2010). Two major modes of variability of the East Asian summer monsoon. *Quarterly Journal of the Royal Meteorological Society*, *136*(649), 829–841. https://doi.org/10.1002/qj.635

Tang, G., Ma, Y., Long, D., Zhong, L., & Hong, Y. (2016). Evaluation of GPM Day-1 IMERG and TMPA Version-7 legacy products over Mainland China at multiple spatiotemporal scales. *Journal of Hydrology*, *533*, 152–167. https://doi.org/10.1016/j.jhydrol.2015.12.008

Tao, S. Y., & Ding, Y. H. (1981). Observational evidence of the influence of the Qinghai-Xizang (Tibet) plateau on the occurrence of heavy rain and severe convective storms in China. *Bulletin of the American Meteorological Society*, *62*(1), 23–30. https://doi.org/10.1175/1520-0477(1981)062<0023:OEOTIO>2.0.CO;2

Wang, C., Chen, G. T.-J., & Carbone, R. E. (2004). A climatology of warm-season cloud patterns over East Asia based on GMS infrared brightness temperature observations. *Monthly Weather Review*, *132*(7), 1606–1629. https://doi.org/10.1175/1520-0493(2004)132<1606:ACOWCP>2.0.CO;2

Wen, L., Zhao, K., Zhang, G., Xue, M., Zhou, B., Liu, S., & Chen, X. (2016). Statistical characteristics of raindrop size distributions observed in East China during the Asian summer monsoon season using 2-D video disdrometer and Micro Rain Radar data. *Journal of Geophysical Research: Atmospheres*, *121*, 2265–2282. https://doi.org/10.1002/2015JD024160

Xu, M., Xu, H., & Ren, H. (2018). Influence of Kuroshio SST front in the East China Sea on the climatological evolution of Meiyu rainband. *Climate Dynamics*, *50*(3-4), 1243–1266. https://doi.org/10.1007/s00382-017-3681-2

Xu, X., Lu, C., Shi, X., & Ding, Y. (2010). Large-scale topography of China: A factor for the seasonal progression of the Meiyu rainband? *Journal of Geophysical Research*, *115*, D02110. https://doi.org/10.1029/2009JD012444

Xue, M., Luo, X., Zhu, K., Sun, Z., & Fei, J. (2018). The controlling role of boundary layer inertial oscillations in Meiyu frontal precipitation and its diurnal cycles over China. *Journal of Geophysical Research: Atmospheres*, *123*, 5090–5115. https://doi.org/10.1029/2018JD028368

Yang, S., & Smith, E. A. (2006). Mechanisms for diurnal variability of global tropical rainfall observed from TRMM. *Journal of Climate*, *19*(20), 5190–5226. https://doi.org/10.1175/JCLI3883.1

Yu, R., & Li, J. (2016). Regional characteristics of diurnal peak phases of precipitation over contiguous China. *Acta Meteorologica Sinca (in Chinese)*, *74*(01), 18–30.

Yu, R., Xu, Y., Zhou, T., & Li, J. (2007). Relation between rainfall duration and diurnal variation in the warm season precipitation over central eastern China. *Geophysical Research Letters*, *34*, L13703. https://doi.org/10.1029/2007GL030315

Yu, R., Zhou, T., Xiong, A., Zhu, Y., & Li, J. (2007). Diurnal variations of summer precipitation over contiguous China. *Geophysical Research Letters*, *34*, L01704. https://doi.org/10.1029/2006GL028129

Zeng, W., Chen, G., du, Y., & Wen, Z. (2019). Diurnal variations of low-level winds and precipitation response to large-scale circulations during a heavy rainfall event. *Monthly Weather Review*, *147*(11), 3981–4004. https://doi.org/10.1175/MWR-D-19-0131.1

Zhang, A., & Fu, Y. (2018). Life cycle effects on the vertical structure of precipitation in East China measured by Himawari-8 and GPM DPR. *Monthly Weather Review*, *146*(7), 2183–2199. https://doi.org/10.1175/MWR-D-18-0085.1

Zhang, A., Fu, Y., Chen, Y., Liu, G., & Zhang, X. (2018). Impact of the surface wind flow on precipitation characteristics over the southern Himalayas: GPM observations. *Atmospheric Research*, *202*, 10–22. https://doi.org/10.1016/j.atmosres.2017.11.001

Zhang, Q., Xu, C. Y., Zhang, Z., Chen, Y. D., Liu, C. L., & Lin, H. (2008). Spatial and temporal variability of precipitation maxima during 1960–2005 in the Yangtze River basin and possible association with large-scale circulation. *Journal of Hydrology*, *353*(3-4), 215–227. https://doi.org/10.1016/j.jhydrol.2007.11.023

Zhang, Y., Xue, M., Zhu, K., & Zhou, B. (2019). What is the main cause of diurnal variation and nocturnal peak of summer precipitation in Sichuan Basin, China? The key role of boundary layer low-level jet inertial oscillations. *Journal of Geophysical Research: Atmospheres*, *124*, 2643–2664. https://doi.org/10.1029/2018JD029834

Zheng, Y., Chen, J., Ge, G., Huang, Y., & Zhang, C. (2008). Review on the synoptic scale Meiyu front system and its synoptics' definition. *Acta Scientiarum Naturalium Universitatis Pekinensis*, *44*(1), 157–164.

Zhou, T., Yu, R., Chen, H., Dai, A., & Pan, Y. (2008). Summer precipitation frequency, intensity, and diurnal cycle over China: A comparison of satellite data with rain gauge observations. *Journal of Climate*, *21*(16), 3997–4010. https://doi.org/10.1175/2008JCLI2028.1

Zhou, T., Yu, R., Zhang, J., Drange, H., Cassou, C., Deser, C., et al. (2009). Why the western Pacific subtropical high has extended westward since the late 1970s. *Journal of Climate*, *22*(8), 2199–2215. https://doi.org/10.1175/2008JCLI2527.1

Zhu, X., Wu, Z., & He, J. (2008). Anomalous Meiyu onset averaged over the Yangtze River valley. *Theoretical and Applied Climatology*, *94*(1-2), 81–95. https://doi.org/10.1007/s00704-007-0347-8